# Emulating Many-Body Localization with a Superconducting Quantum Processor

Kai Xu,[1] Jin-Jun Chen,[2,3] Yu Zeng,[2,3] Yu-Ran Zhang,[2,3] Chao Song,[1] Wuxin Liu,[1] Qiujiang Guo,[1] Pengfei Zhang,[1] Da Xu,[1] Hui Deng,[2] Keqiang Huang,[2,3] H. Wang,[1,4,*] Xiaobo Zhu,[4,†] Dongning Zheng,[2,3] and Heng Fan[2,3,‡]

[1]*Department of Physics, Zhejiang University, Hangzhou, Zhejiang 310027, China*

[2]*Beijing National Laboratory for Condensed Matter Physics, Institute of Physics, Chinese Academy of Sciences, Beijing 100190, China*

[3]*School of Physical Sciences, University of Chinese Academy of Sciences, Beijing 100049, China*

[4]*Synergetic Innovation Centre in Quantum Information and Quantum Physics, University of Science and Technology of China, Hefei, Anhui 230026, China*

(Received 1 October 2017; published 2 February 2018)

The law of statistical physics dictates that generic closed quantum many-body systems initialized in nonequilibrium will thermalize under their own dynamics. However, the emergence of many-body localization (MBL) owing to the interplay between interaction and disorder, which is in stark contrast to Anderson localization, which only addresses noninteracting particles in the presence of disorder, greatly challenges this concept, because it prevents the systems from evolving to the ergodic thermalized state. One critical evidence of MBL is the long-time logarithmic growth of entanglement entropy, and a direct observation of it is still elusive due to the experimental challenges in multiqubit single-shot measurement and quantum state tomography. Here we present an experiment fully emulating the MBL dynamics with a 10-qubit superconducting quantum processor, which represents a spin-1/2 $XY$ model featuring programmable disorder and long-range spin-spin interactions. We provide essential signatures of MBL, such as the imbalance due to the initial nonequilibrium, the violation of eigenstate thermalization hypothesis, and, more importantly, the direct evidence of the long-time logarithmic growth of entanglement entropy. Our results lay solid foundations for precisely simulating the intriguing physics of quantum many-body systems on the platform of large-scale multiqubit superconducting quantum processors.

DOI: 10.1103/PhysRevLett.120.050507

*Introduction.*—A central assumption of statistical mechanics is that generic closed quantum systems driven out of equilibrium will thermalize to the ergodic state, which has no quantum correlations [1–4]. One exception was demonstrated by Anderson [5], who argued that disordered systems featuring single-particle localization, known as Anderson localization, can fail to thermalize. Systems exhibiting Anderson localization require noninteracting particles with low excitation energies and have been widely studied in a number of works [6–12]. However, in quantum many-body systems featuring interacting particles and high energy excitations where Anderson localization is no longer applicable, there emerges a new phase of localization, many-body localization (MBL) [13], which also prevents the systems from thermalizing and breaks down ergodicity. The MBL phase resembles the Anderson localization phase in that both phases explicitly go against the eigenstate thermalization hypothesis (ETH), which implies that entanglement entropy violates volume law [14,15]. Nevertheless, the MBL phase has very different dynamical properties [16], and a unique signature of MBL is the long-time logarithmic growth of entanglement entropy, which correlates with a slow evolution toward equilibrium as resulting from dephasing caused by interactions between particles [17–20].

Recent experimental progresses have allowed the realization of MBL in a controllable manner on various artificially engineered platforms, which have facilitated the detailed investigations of thermalization and MBL in quantum many-body systems covering a wide range of aspects, such as the emergence of the disorder-induced insulating state [21], the breaking down of ergodicity [22], the difference between Anderson localization and MBL in optical lattice [23], and the localization-delocalization transition in a three-dimensional system with nuclear magnetic resonance [24]. Moreover, the long-time logarithmic growth of entanglement entropy, the hallmark of MBL, is indirectly shown by measuring the quantum Fisher information in a disordered spin chain with ten trapped ions [25]. However, a direct observation of the MBL hallmark requires the capability of performing fast and accurate quantum state tomography (QST) on the many-body system, which has yet to be achieved.

Here we present an experiment of fully emulating the MBL dynamics with a superconducting quantum processor, which represents a spin-1/2 $XY$ model featuring tunable disorder and long-range spin-spin interactions. Our processor chip integrates ten frequency-tunable transmon qubits that are interconnected by a central bus resonator $\mathcal{R}$, with the circuit architecture introduced in Fig. 1 and elsewhere [26]. Some prominent characteristics of this experimental platform for MBL are as follows. First, the frequency and the state of each qubit can be individually

 

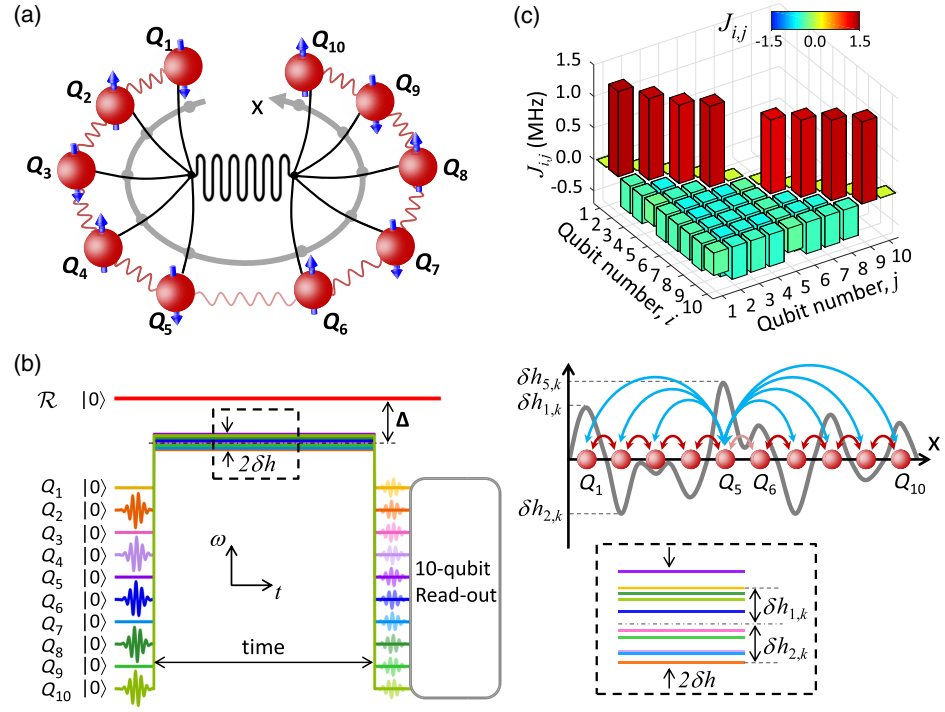


FIG. 1. Experimental setup. (a) Diagram of the 10-qubit superconducting quantum processor. The qubits, shown as atoms with spins initialized in alternate orientations, are arranged along a circular chain with the nearest-neighbor couplings represented by red wavy lines, which are calibrated in a separate measurement as discussed in the Supplemental Material (the coupling for $Q_5$ and $Q_6$ is smaller than others) [35]. The long-range, i.e., beyond nearest-neighbor, spin-spin interactions are enabled by the central bus resonator $\mathcal{R}$ that couples to each individual qubit as illustrated by curved connecting lines. (b) Pulse sequences for emulating MBL. All ten qubits are initialized at their respective idle frequencies by applying $\pi$ pulses (dark-color sinusoids) to the even-site qubits to prepare the initial state $|0101010101\rangle$, following which the rectangular pulses are applied to quickly bias all qubits to nearby $\Delta/2\pi = -650$ MHz. Individual $Q_i$ is offset from $\Delta$ by a small amount of $\delta h_{i,k} \in [-\delta h, \delta h]$, where $\delta h_{i,k}$ is randomly chosen but fixed for the $k$th pulse sequence (see the bottom right panel for the enlarged view of the pulse segment enclosed by dashed lines), and the ensemble of the $k = 1$–30 pulse sequences effectively emulates the random disordered potential $\delta h_i$. After the 10-qubit system evolves for a specific time from 0 to 1000 ns under the square pulses, all qubits are biased back to their respective idle frequencies for the 10-qubit joint read-out, which returns binary outcomes of the ten qubits: We run all the $k = 1$–30 sequences, each being executed for 3000 times, to count $2^{10}$ probabilities of $\{P_{00\ldots0}, P_{00\ldots1}, \ldots, P_{11\ldots1}\}_k$ for $k = 1$–30. Mean of the $k = 1$–30 probability ensemble captures the effect of the random disorder. If the $N$-qubit QST is necessary, we insert tomographic rotation pulses (light-color sinusoids) to the involved qubits before the $N$-qubit joint read-out to obtain all tomographic probabilities, $3^N$ more than aforesaid, to calculate the $N$-qubit density matrix for the $k$th sequence. (Top right) The circular spin chain arranged in one dimension for illustrating the quantity $\delta h_{i,k}$. (c) The spin-spin coupling matrix $J_{ij}$ for $\Delta/2\pi = -650$ MHz. Only nearest-neighbor couplings are positive, while all other interaction terms are negative, which do not decay over distance.

manipulated via its own control lines, and the qubit-qubit interaction within an arbitrary two-qubit pair can be mediated by detuning their frequency from that of the resonator $\mathcal{R}$, so that both the disorder and the long-range interactions are programmable. This is a necessary condition for MBL since the $XY$ model becomes nonintegrable with the nonvanishing long-range interactions. Second, the fast and accurate QST as demonstrated for up to ten superconducting qubits in Ref. [26] allows us to record the dynamics of entanglement entropy, making it possible for observing the aforesaid MBL hallmark. Third, with the recent advances in coherence, scalability, and controllability for superconducting quantum circuits [26–33], the platform becomes well suited for simulating and exploring MBL and other intriguing but intractable questions of quantum many-body systems [34].

*Hamiltonian.*—In our superconducting quantum processor, the resonator mediated superexchange interactions within arbitrary two-qubit pairs give an effective Hamiltonian as (see Fig. 1, Ref. [26], and Supplemental Material [35]),

$$\frac{H}{\hbar} = \sum_{i<j} J_{ij}(\sigma_i^+\sigma_j^- + \sigma_i^-\sigma_j^+) + \sum_i (h_i + \delta h_i)\sigma_i^+\sigma_i^-, \quad (1)$$

where $\sigma_i^{\pm}$ are the raising (lowering) operators, $h_i$ is the strength of the inherent transverse magnetic field, $\delta h_i$ is the random disordered potential of the $i$th spin, and $J_{ij}$ is the

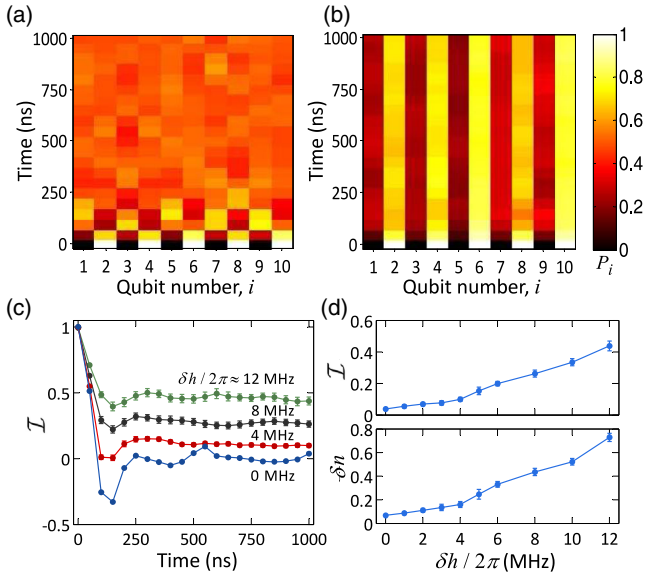


FIG. 2. Dynamics of imbalance for the system initialized in $|0101010101\rangle$. (a),(b) The time evolutions of the excited-state ($|1\rangle$-state) probabilities $P_i$ (color bar on the far right) for $Q_i$ (indexed as qubit number $i$) when there is no disorder with $\delta h \approx 0$ and a strong disorder with $\delta h/2\pi \approx 12$ MHz, respectively. All probabilities are after read-out correction [40]. (c) Time evolutions of the system imbalance $\mathcal{I}$ at different disorder strengths $\delta h$ as listed. (d) The quasi-steady-state imbalance $\mathcal{I}$ (top) and standard deviation $\delta n$ of the $|1\rangle$-state probability distributions taken at 1000 ns as functions of $\delta h$, showing that the system thermalizes for no disorder, but starts to enter the MBL phase with increasing disorder strength. Error bars are 1 SD calculated from all probability data of the $k = 1$–30 pulse sequences. The transition looks a bit continuous for our 10-qubit system, but numerical simulations involving up to 20 qubits show that it becomes more pronounced and the associated critical disorder strength can be identified when the qubit number increases.

coupling strength between the $i$th and $j$th spins. The Hamiltonian is an effective $XY$ model, which conserves the total number of spin excitations [39].

As shown in Fig. 1, $J_{ij}$ contains two parts, the nearest-neighbor direct coupling term $\lambda^{c}_{i,i+1}$, and the superexchange interaction $J^{SE}_{ij}$. Most $\lambda^{c}_{i,i+1}/2\pi$ are around 1.8 MHz (see Supplemental Material [35]), which play a leading role compared with the corresponding superexchange interactions. The superexchange interaction $J^{SE}_{ij}$ between arbitrary two qubits $Q_i$ and $Q_j$ arises only if the two qubits are biased to the same detuning, i.e., $\Delta_i = \Delta_j$, with a magnitude $\propto 1/\Delta_i$. In this experiment, all qubits are detuned to $\Delta/2\pi \approx -650$ MHz; therefore, $J^{SE}_{ij}/2\pi$ range from $-0.33$ to $-0.64$ MHz. The spin-spin coupling matrix $J_{ij}$ is shown in Fig. 1(c). The inherent magnetic field strength $h_i$ ($\propto 1/\Delta_i$) remains constant in the experiment (see Ref. [26] and Supplemental Material [35]). $\delta h_i$ denotes the on site disordered potential taken from a uniform random distribution with $\delta h_i \in [-\delta h, \delta h]$. This disorder is generated by applying the frequency shift of $\delta h_i$ to $Q_i$, for $i = 1$–10, on top of the large detuning $\Delta$, where $\delta h \ll \Delta$, so that the coupling matrix $J_{ij}$ in Fig. 1(c) remains invariant. Experimentally, evolution of the system toward either thermalization or the MBL phase is controlled by the disorder strength $\delta h$ (see Fig. 1).

*Imbalance.*—Emergence of imbalance and ergodicity breaking are important signatures for the system crossing from the thermalized phase to the MBL phase. In the experiment, we initialize the system by preparing a 10-qubit Néel ordered state, $|\psi_0\rangle = |0101010101\rangle$, with $|0\rangle$ representing the ground state of a qubit on odd number sites and $|1\rangle$ representing the excited state on even number sites. We study the ergodic properties via tracing the system imbalance due to the Néel nonequilibrium, defined as $\mathcal{I} = [(N_e - N_o)/(N_e + N_o)]$, where $N_e$ ($N_o$) is the total number of excitation quanta on the even (odd) number sites.

We apply the pulse sequence as shown in Fig. 1(b) and record the system dynamics with the 10-qubit joint read-out. At long times around 250 ns or above, the system reaches a quasisteady state. Figures 2(a) and 2(b) show the time evolutions of the $|1\rangle$-state probabilities of individual qubits, which approach 0.5 for all qubit sites after $t \approx$ 250 ns in the absence of disorder, but maintain almost the original values in the presence of a strong disorder ($\delta h/2\pi \approx 12$ MHz). In Fig. 2(c), it is seen that imbalance $\mathcal{I}$ reaches a quasi-steady-state value at ≈250 ns for all disorder strengths. The quasi-steady-state $\mathcal{I}$ is zero for $\delta h \approx 0$, but remains nonzero and becomes larger as the disorder strength increases, signaling the entrance to the

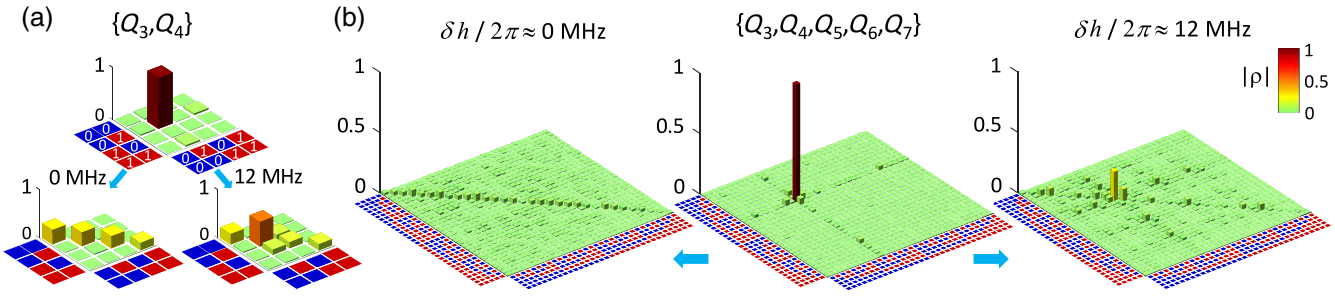


FIG. 3. Subsystem density matrices for test of ETH. Shown are the experimental initial density matrices in absolute value for the 2-qubit subsystems in (a) and 5-qubit subsystems in (b), in comparison with those probed at 1000 ns when the system evolves to either the thermalized state ($\delta h \approx 0$) or the MBL phase ($\delta h/2\pi \approx 12$ MHz). Density matrix data of the 1-qubit subsystem $Q_3$ at a few selected evolution times can be found in the Supplemental Material [35].

MBL phase that breaks down ergodicity. The maximum evolution time is much shorter than the qubit coherence times, and we have postselected the qubit probabilities that conserve the total excitations to guarantee that our experimental system is an effectively closed quantum system (see Supplemental Material [35]).

The quasi-steady-state imbalance can be taken as an order parameter to quantify the crossover from the ergodic thermal phase to the nonergodic MBL phase tuned by the disorder strength $\delta h$, as shown in Fig. 2(d). We also measure the standard deviation $\delta n = \sqrt{\sum_{i=1}^{10}[P_i(0) - P_i(\delta h)]^2}$ of the $|1\rangle$-state probability distributions between the ideal thermal state with $P_i(0) = 0.5$, for $i = 1$–10, and the quasisteady state as a function of the disorder strength $\delta h$, which works as a sensitive detector to witness the crossover.

*Eigenstate thermalization hypothesis.*—In the absence of disorder, the initial Néel state evolves to the thermal state, which satisfies ETH and ensures that any resulting subsystem is a completely mixed state described by a generalized Gibbs ensemble with an infinite temperature (see Supplemental Material [35]). In contrast, in the presence of a strong disorder, ETH fails and the reduced density matrix of an arbitrary subsystem retains the initial form.

Using the multiqubit QST, we show in Fig. 3 the averaged norms of the subsystem density matrices at 0 and 1000 ns for two cases: one in the absence of disorder with $\delta h \approx 0$ and the other in the presence of a strong disorder with $\delta h/2\pi \approx 12$ MHz. For subsystems with one, two, and five qubits, the experimental data all agree reasonably well with the expected thermal equilibrium when $\delta h \approx 0$, but retain the initial form when $\delta h/2\pi \approx 12$ MHz, the latter of which clearly violates ETH.

*Entanglement entropy.*—The dynamics of entanglement entropy for an isolated system is a well-defined signature for differentiating between thermalization, Anderson localization, and MBL. Here we focus on the evolution of the half-chain entanglement entropy using QST for the system initialized in the Néel ordered state. With interparticle interactions but no disorder, the system is quickly thermalized and its entanglement entropy saturates to the maximum (thermal) entropy that depends on the system size and satisfies volume law [4]. With strong disorder but no interparticle interactions, there arises Anderson localization, and entanglement entropy quickly saturates to a constant that is independent of the system size and much smaller than the maximum entropy [19]. With both strong disorder and interparticle interactions, the system enters the MBL phase, where the disorder prevents the particle transport and leads to a slow growth of entanglement entropy compared with that of the thermal phase, but the interparticle interactions contribute to the transport of phase correlations so that entanglement entropy persistently increases logarithmically in time compared with that of Anderson localization [17–19,41,42].

For a realistic quantum system, decoherence has to be taken into account, and the influence of dissipation on MBL has been investigated in Refs. [20,43]. Without loss of generality, here we quote the five qubits $\{Q_3, Q_4, Q_5, Q_6, Q_7\}$ as subsystem $A$ and the rest of the qubits as subsystem $B$ and study the evolution of the half-chain entanglement entropy $S = -\mathrm{tr}(\rho_A \ln \rho_A)$, where $\rho_A$ is the reduced density operator of subsystem $A$ by tracing out the subsystem $B$ (see Supplemental Material [35] for a similar set of experimental data with another choice of the subsystems).

Figures 4(a) and 4(b) show the time evolutions of the half-chain entanglement entropy at different disorder

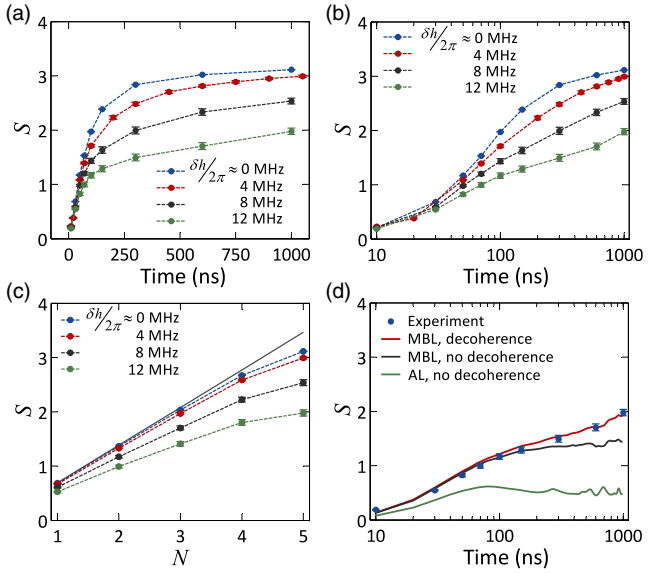


FIG. 4. Half-chain entanglement entropy for the 5-qubit subsystem $\{Q_3, Q_4, Q_5, Q_6, Q_7\}$, of which the density matrices are obtained by QST. (a),(b) The entanglement entropy $S$ as functions of the evolution time, in linear scale and in logarithmic scale, respectively, at different disorder strengths $\delta h$ as labeled. (c) Site-averaged $S$ at around 1000 ns as functions of the number of sites (qubits) $N$ at different disorder strengths $\delta h$ as indicated, which are calculated by taking the average of the entanglement entropies of all $N$-site choices ($N \leq 5$) out of the directly measured 5-qubit subsystem. Dots connected by dashed lines are experimental data. The solid line shows $S = N \ln 2$. (d) Entanglement entropy $S$ as functions of the evolution time for comparison between MBL and Anderson localization (AL) with the disorder strength $\delta h/2\pi \approx 12$ MHz. Dots are experimental data, and lines are numerical simulation results as indicated (see Supplemental Material [35]). Error bars are 1 SD calculated from all tomography data of the $k = 1$–30 pulse sequences. Since there is no straightforward method for calculating the entanglement entropy $S$ of a mixed state [44], here we estimate $S$ using the subsystem density matrix with the assumption that the 10-qubit system remains in a pure state. The apparent increase of $S$ under decoherence is due to an imperfection of such a pure-state assumption. We further verify with numerical simulations that the residual excited state population in each qubit, typically 0.01 or less due to unwanted excitations [26], has minimal impact on the signature of the long-time logarithmic growth of $S$ in the MBL phase.

strengths as indicated. As expected, for all disorder strengths, $S$ grows quickly and linearly in time at the beginning and then enters a slow growth period. For strong disorder strengths such as $\delta h/2\pi \approx 8$ and 12 MHz, $S$ appears to grow logarithmically in time during the whole process. Figure 4(c) shows the site-averaged entanglement entropy at ≈1000 ns as functions of the number of sites $N$ for different disorder strengths. For $\delta h \approx 0$ and $N \leq 4$, the site-averaged entanglement entropy is close to thermal entropy $N \ln 2$, which satisfies volume law. However, for strong disorder such as $\delta h/2\pi \approx 12$ MHz, it falls significantly below thermal entropy and therefore violates volume law. Figure 4(d) shows the difference between MBL and Anderson localization. When the coupling strengths $J_{ij}$ contain only nearest-neighbor terms, the Hamiltonian in Eq. (1) can be mapped to a noninteracting fermionic model (see Supplemental Material [35]) and the strong disorder gives rise to Anderson localization, where entanglement entropy saturates quickly (green line). In contrast, the MBL phase demonstrates the long-time logarithmic growth of entanglement entropy, as directly observed experimentally (dots), which is in excellent agreement with the numerical simulation taking into account decoherence (red line).

In conclusion, we have presented key evidence for MBL and thermalization in a long-range interacting many-body system controllably induced by strong disorder and no disorder, respectively. Our implementation is based on a 10-qubit superconducting quantum processor, which provides tunable disorder and all-to-all qubit-qubit interactions. The interactions do not decay over distance and thus are nonlocal, so that the MBL phase achieved in our setup can be viewed as supplemental to the generally studied "finite range" situation [45]. Furthermore, we have directly observed the long-time logarithmic growth of entanglement entropy, the hallmark of the MBL phase. Our demonstration shows that superconducting quantum processors can work precisely in simulating various intriguing phenomena of quantum many-body systems.

This work was supported by the National Basic Research Program of China (Grants No. 2014CB921201, No. 2016YFA0302104, No. 2014CB921401, and No. 2016YFA0300600), the National Natural Science Foundations of China (Grants No. 11434008, No. 91536108, No. 91321208, and No. 11574380), Chinese Academy of Sciences Center for Excellence in Topological Quantum Computation (Grant No. XDPB08-3), and the Fundamental Research Funds for the Central Universities of China (Grant No. 2016XZZX002-01). Devices were made at the Nanofabrication Facilities at Institute of Physics in Beijing, University of Science and Technology of China in Hefei, and National Center for Nanoscience and Technology in Beijing.

K. X. and J.-J. C. contributed equally to this work.

*hhwang@zju.edu.cn
†xbzhu16@ustc.edu.cn
‡hfan@iphy.ac.cn

[1] J. M. Deutsch, Phys. Rev. A **43**, 2046 (1991).
[2] M. Srednicki, Phys. Rev. E **50**, 888 (1994).
[3] M. Rigol, V. Dunjko, and M. Olshanii, Nature (London) **452**, 854 (2008).
[4] C. Gogolin and J. Eisert, Rep. Prog. Phys. **79**, 056001 (2016).
[5] P. W. Anderson, Phys. Rev. **109**, 1492 (1958).
[6] D. S. Wiersma, P. Bartolini, A. Lagendijk, and R. Righini, Nature (London) **390**, 671 (1997).
[7] R. Dalichaouch, J. P. Armstrong, S. Schultz, P. M. Platzman, and S. L. McCall, Nature (London) **354**, 53 (1991).
[8] F. Scheffold, R. Lenke, R. Tweer, and G. Maret, Nature (London) **398**, 206 (1999).
[9] A. A. Chabanov, M. Stoytchev, and A. Z. Genack, Nature (London) **404**, 850 (2000).
[10] T. Schwartz, G. Bartal, S. Fishman, and M. Segev, Nature (London) **446**, 52 (2007).
[11] S. S. Kondov, W. R. McGehee, J. J. Zirbel, and B. DeMarco, Science **334**, 66 (2011).
[12] Y. Chen *et al.*, Nat. Commun. **5**, 5184 (2014).
[13] D. M. Basko, I. L. Aleiner, and B. L. Altshuler, Ann. Phys. (Amsterdam) **321**, 1126 (2006).
[14] J. A. Kjäll, J. H. Bardarson, and F. Pollmann, Phys. Rev. Lett. **113**, 107204 (2014).
[15] R. Nandkishore and D. A. Huse, Annu. Rev. Condens. Matter Phys. **6**, 15 (2015).
[16] M. Serbyn, M. Knap, S. Gopalakrishnan, Z. Papić, N. Y. Yao, C. R. Laumann, D. A. Abanin, M. D. Lukin, and E. A. Demler, Phys. Rev. Lett. **113**, 147204 (2014).
[17] M. Žnidarič, T. Prosen, and P. Prelovšek, Phys. Rev. B **77**, 064426 (2008).
[18] P. Ponte, Z. Papić, F. Huveneers, and D. A. Abanin, Phys. Rev. Lett. **114**, 140401 (2015).
[19] R. Modak and S. Mukerjee, Phys. Rev. Lett. **115**, 230401 (2015).
[20] E. Levi, M. Heyl, I. Lesanovsky, and J. P. Garrahan, Phys. Rev. Lett. **116**, 237203 (2016).
[21] S. Kondov, W. McGehee, W. Xu, and B. DeMarco, Phys. Rev. Lett. **114**, 083002 (2015).
[22] M. Schreiber, S. S. Hodgman, P. Bordia, H. P. Lüschen, M. H. Fischer, R. Vosk, E. Altman, U. Schneider, and I. Bloch, Science **349**, 842 (2015).
[23] P. Bordia, H. P. Luschen, S. S. Hodgman, M. Schreiber, I. Bloch, and U. Schneider, Phys. Rev. Lett. **116**, 140401 (2016).
[24] G. A. Álvarez, D. Suter, and R. Kaiser, Science **349**, 846 (2015).
[25] J. Smith, A. Lee, P. Richerme, B. Neyenhuis, P. W. Hess, P. Hauke, M. Heyl, D. A. Huse, and C. Monroe, Nat. Phys. **12**, 907 (2016).
[26] C. Song *et al.*, Phys. Rev. Lett. **119**, 180511 (2017).
[27] L. DiCarlo *et al.*, Nature (London) **460**, 240 (2009).
[28] M. Mariantoni *et al.*, Science **334**, 61 (2011).
[29] A. Fedorov, L. Steffen, M. Baur, M. P. da Silva, and A. Wallraff, Nature (London) **481**, 170 (2012).
[30] R. Barends *et al.*, Nature (London) **508**, 500 (2014).
[31] D. Ristè, S. Poletto, M.-Z. Huang, A. Bruno, V. Vesterinen, O.-P. Saira, and L. DiCarlo, Nat. Commun. **6**, 6983 (2015).

[32] M. Takita, A. D. Córcoles, E. Magesan, B. Abdo, M. Brink, A. Cross, J. M. Chow, and J. M. Gambetta, Phys. Rev. Lett. **117**, 210505 (2016).
[33] D. Rosenberg *et al.*, npj Quantum Inf. **3**, 42 (2017).
[34] I. M. Georgescu, S. Ashhab, and F. Nori, Rev. Mod. Phys. **86**, 153 (2014).
[35] See Supplemental Material at http://link.aps.org/supplemental/10.1103/PhysRevLett.120.050507 for more information on the device and more experimental data supporting the existence of the MBL phase, which includes Refs. [36–38].
[36] E. H. Lieb and D. W. Robinson, Commun. Math. Phys. **28**, 251 (1972).
[37] H. Tasaki, Phys. Rev. Lett. **80**, 1373 (1998).
[38] E. Lieb, T. Schultz, and D. Mattis, Ann. Phys. (N.Y.) **16**, 407 (1961).
[39] P. Jurcevic, B. P. Lanyon, P. Hauke, C. Hempel, P. Zoller, R. Blatt, and C. F. Roos, Nature (London) **511**, 202 (2014).
[40] Y. Zheng *et al.*, Phys. Rev. Lett. **118**, 210504 (2017).
[41] J. H. Bardarson, F. Pollmann, and J. E. Moore, Phys. Rev. Lett. **109**, 017202 (2012).
[42] M. Pino, Phys. Rev. B **90**, 174204 (2014).
[43] M. V. Medvedyeva, T. Prosen, and M. Žnidarič, Phys. Rev. B **93**, 094205 (2016).
[44] R. Horodecki, P. Horodecki, M. Horodecki, and K. Horodecki, Rev. Mod. Phys. **81**, 865 (2009).
[45] M. B. Hastings, in *Quantum Theory from Small to Large Scales* Lecture Notes of the Les Houches Summer School, Vol. 95 (Oxford University Press, New York, 2010) p. 171.